Volume 10 | Number 24 | 28 June 2014 | Pages 4219–4414

# Soft Matter

www.softmatter.org

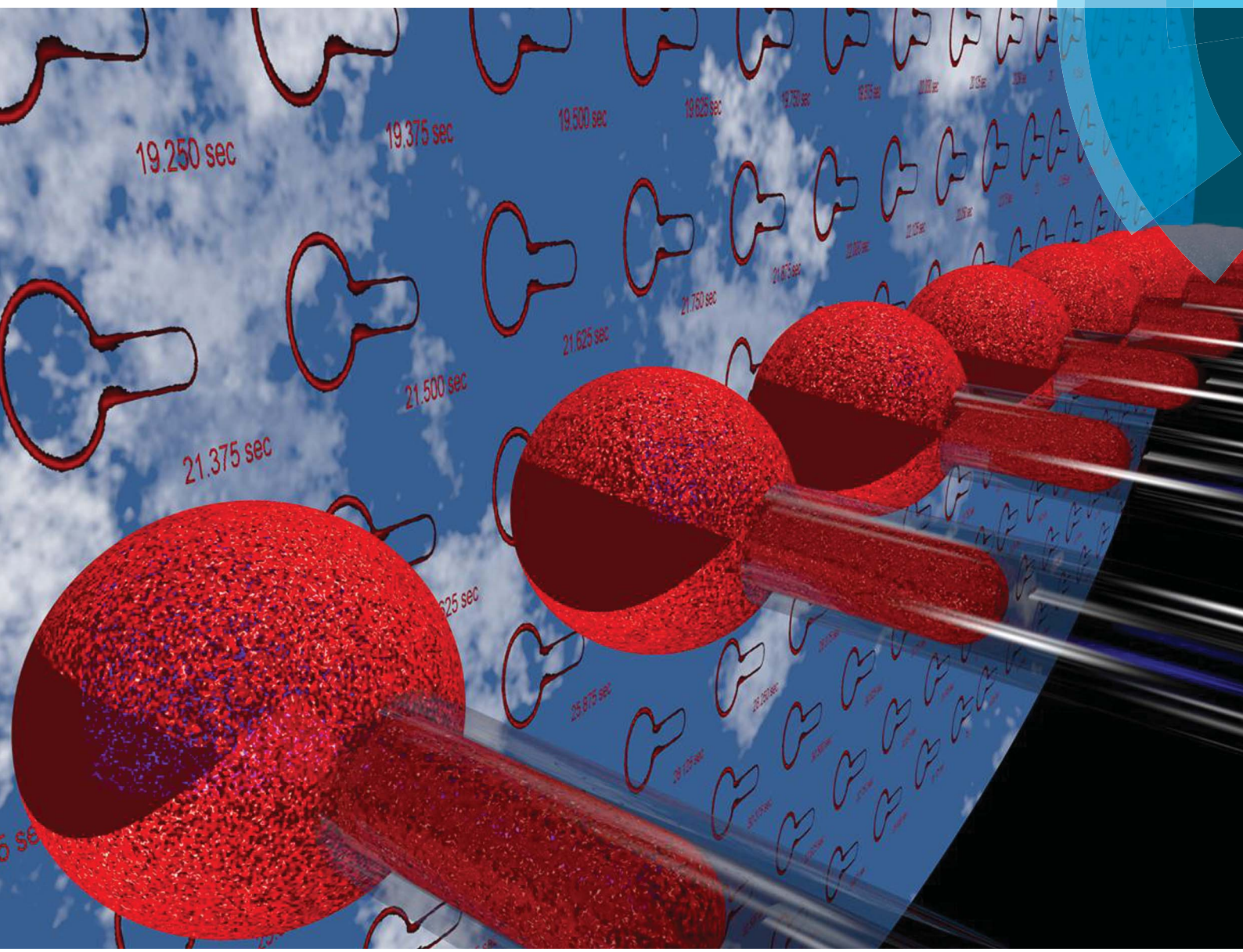


ISSN 1744-683X

ROYAL SOCIETY OF CHEMISTRY

PAPER
Carlos M. Marques *et al.*
Lipid oxidation induces structural changes in biomimetic membranes

Soft Matter

PAPER

# Lipid oxidation induces structural changes in biomimetic membranes†

Cite this: *Soft Matter*, 2014, **10**, 4241

Georges Weber,[a] Thierry Charitat,[b] Maurício S. Baptista,[c] Adjaci F. Uchoa,[c] Christiane Pavani,[c] Helena C. Junqueira,[d] Yachong Guo,[d] Vladimir A. Baulin,[e] Rosangela Itri,[d] Carlos M. Marques*[b] and André P. Schroder[b]

Received 28th October 2013
Accepted 20th December 2013

DOI: 10.1039/c3sm52740a

www.rsc.org/softmatter

Oxidation can intimately influence and structurally compromise the levels of biological self-assembly embodied by intracellular and plasma membranes. Lipid peroxidation, a natural metabolic outcome of life with oxygen under light, is also a salient oxidation reaction in photomedicine treatments. However, the effect of peroxidation on the fate of lipid membranes remains elusive. Here we use a new photosensitizer that anchors and disperses in the membrane to achieve spatial control of the oxidizing species. We find, surprisingly, that the integrity of unsaturated unilamellar vesicles is preserved even for fully oxidized membranes. Membrane survival allows for the quantification of the transformations of the peroxidized bilayers, providing key physical and chemical information to understand the effect of lipid oxidation on protein insertion and on other mechanisms of cell function. We anticipate that spatially controlled oxidation will emerge as a new powerful strategy for tuning and evaluating lipid membranes in biomimetic media under oxidative stress.

## 1 Introduction

Lipid oxidation plays a central role in the life of the eukaryotic cells, where it is a direct consequence of the reactive oxygen species generated not only by mitochondrial respiration, but also by many other processes such as inflammation, catalysis by peroxisomal oxidases, virus phagocytosis, ultraviolet and ionic irradiation, to name only a few.[1–3] A controlled amount of oxidized lipids is required for cell signaling, cell maturation and differentiation, and cell apoptosis. However, the products of lipid oxidation, if uncontrolled, can have a deleterious effect on the functioning of the cell, and are known to be involved in a variety of diseases including Parkinson's and Alzheimer's neuro-degenerations, hypertension and cancer.[4,5] Lipid oxidation is also key to photodynamic therapy or PDT, a technique clinically used in pathologies such as skin or oesophagus cancer, where tumors are destroyed by intense light-induced tissue oxidation.[6–8]

In biological media, photo-induced oxidation is often initiated by light activation of a photosensitizer into its triplet state. In the so-called type II reactions, quenching of this triplet state by molecular oxygen $O_2$ leads to the formation of singlet oxygen $^1O_2$, a highly reactive species that diffuses in aqueous solutions over a distance of $\ell_D \simeq 100$ nm before it decays.[9] Given that the prime targets for oxidation in lipid bilayers are the unsaturated sites along the alkyl chains, an efficient distribution for the $^1O_2$ sources requires the dyes to be within a distance $\ell_D$ from the membranes. In the absence of transition metals the reaction of a singlet oxygen with a double bond leads only to the formation of the organic hydroperoxide group –OOH.[10,11] However, the direct type I reactions between the triplet state of an activated photosensitizer and the chain double bonds can also initiate chain reactions with intermediate lipid radicals, leading eventually to secondary peroxidized lipid products like alcohols, aldehydes, ketones and lactones.[12] A key requirement in designing model systems to study oxidation of lipid membranes mediated by singlet oxygen is therefore to achieve an appropriate spatial distribution of photosensitizers, a distribution that not only brings singlet oxygen sources to within $\ell_D$ of the bilayer but also precisely controls the probability of a direct encounter between the photosensitizer and the unsaturated bond.[13]

In this paper we study DOPC and POPC giant vesicles decorated by a new amphiphilic chlorin photosensitizer with an added scaffold that anchors well in the membranes yet

[a]*Present address: FOM Institute AMOLF, Science Park 104, 1098 XG Amsterdam, The Netherlands*

[b]*Université de Strasbourg, Institut Charles Sadron, CNRS, 23 Rue du Loess, BP 84047, 67034 Strasbourg Cedex 2, France. E-mail: marques@unistra.fr; Fax: +33 3 8841 4099; Tel: +33 3 8841 4045*

[c]*Departamento de Bioquímica, Instituto de Química, Universidade de São Paulo, 05508-000, São Paulo, Brazil*

[d]*Departamento de Física Aplicada, Instituto de Física, Universidade de São Paulo, CP 66318, 05314970, São Paulo, Brazil*

[e]*Departament d'Enginyeria Química, Universitat Rovira i Virgili, Av. dels Països Catalans, 26, Tarragona 43007, Spain*

† Electronic supplementary information (ESI) available. See DOI: 10.1039/c3sm52740a

preventing aggregation.[14] Changes in permeability, fluidity, packing order or thickness in model lipid bilayers, as well as vesicle destruction, have been reported elsewhere,[15–20] without however achieving spatial localization of the oxidizing centers or a precise control of the chemical oxidation processes at play. Here, by anchoring the photosensitizing agent on the membrane we were able to induce exclusive hydroperoxidation of the lipids while preserving membrane integrity. Under such conditions, the associated molecular and mechanical changes could be precisely measured and further compared with theoretical predictions from Single Chain Mean Field (SCMF) theory for lipid bilayers.[21]

## 2 Experimental section

### 2.1 Phospholipids and reagents

The phospholipids, 1-palmitoyl-2-oleoyl-*sn-glycero*-3-phosphocholine (POPC) and 1,2-dioleoyl-*sn-glycero*-3-phosphocholine (DOPC) and all other chemicals were purchased from Sigma-Aldrich.

### 2.2 The photosensitizer

**Synthesis and characterization.** The photosensitizer Chlorin-12 was synthesized with protoporphyrin IX diester (42.3 mmol) and excess of 4-dodecylphenyl maleimide, by Diels–Alder reactions according to the procedure described in the literature.[14] It was purified using column chromatography (silica) followed by preparative TLC (silica), using a 50 : 1 mixture of $CHCl_3$–AcOEt as eluant, which furnished two pure isomers. The two isomers have an $R_f$ of 0.55 and 0.68, the combined product of both isomers yields 72% (29.6 mmol). The compound that we named Chlorin-12 – see Fig. 1 – was the second of the isomers characterized by $^1$H-NMR, COSY, ESI-MS and UV-Vis spectroscopy – see ESI.† ESI-MS-TOF, *m*/*z* 933.5321 was calculated for $C_{58}H_{70}N_5O_6^+$ ($MH^+$); found 933.5329.

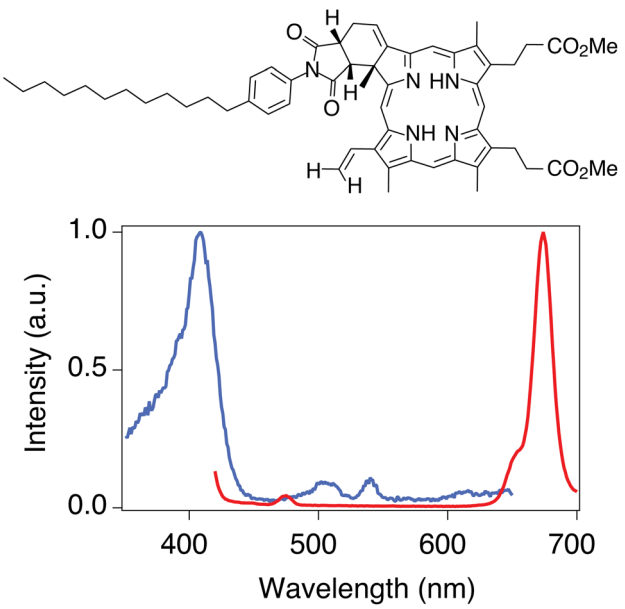


Fig. 1 Chemical structure of the new photosensitizer Chlorin-12 and its absorption and emission spectra for solutions of POPC liposomes decorated with Chlorin-12.

**Quantum yield.** Quantum yield was measured by anchoring 1% Chlorin-12 in POPC liposomes. The two components were first diluted at the desired composition in chloroform, then spread onto a test tube. After letting the solvent evaporate, the film was hydrated in $D_2O$. The resulting opalescent solution was sonicated (seven cycles of thirty seconds sonication with thirty seconds rest, cooled in an ice bath, with tip sonicator operating at 20–30 W), leading to an opalescent solution that was studied with dynamic light scattering. The results exhibited a narrow hydrodynamic radius of 100 nm for the liposomes in the solution.

The detection of the near infrared emission of the singlet oxygen molecule at 1270 nm is a standard method to determine $^1O_2$ quantum yield $\phi_\Delta$. Both the liposome solution and the acetonitrile solution of Chlorin-12 that was used as a standard ($\phi_\Delta = 0.7$) exhibit an absorbance value close to 0.02 (1 cm path length) at 640 nm. A Continuum Surelite III Nd:YAG laser was used as the excitation source operating at 532 nm (5 ns, 10 Hz) to pump a dye laser (DCM 2-(2-(4-(dimethylamino)phenyl)-6-methyl-4*H*-pyran-4-ylidene)propanedinitrile in ethanol) emitting at 640 nm. The singlet oxygen emission at 1270 nm was detected at right angle in a liquid nitrogen cooled photomultiplier (Hamamatsu R5509). The value $\phi_\Delta = 0.63$ was calculated by measuring and comparing the emissions of sample and standard, correcting also for the refraction index differences (acetonitrile 1.344, deuterium oxide 1.328) and for the $^1O_2$ lifetimes (acetonitrile 60 μs, liposomes in deuterium oxide 16 μs).[22]

**Amphiphilic behavior.** Chlorin-12 has an amphiphilic character that can be clearly demonstrated by performing Langmuir isotherms[23] (Langmuir trough, Nima). At the air–water interface, a stable film is formed and compression isotherms show standard monolayer behaviour for pressures in the range of 5–40 mN $m^{-1}$, as shown in the ESI†.

**Preparation of the hydroperoxidized form of POPC.** The hydroperoxide form of POPC, that we designate by POPC–OOH, was produced through irradiation of POPC in methylene blue (MB) solution as follows. 80 mg of POPC was dissolved in 5 mL of chloroform, to which 1 mL of a 0.3 mM methanol solution of MB was added. This mixture was kept in an ice bath and stirred continuously. The irradiation was performed with a tungsten lamp (500 W) for 8 h. The mixture of solvent was evaporated and 1 mL of methanol HPLC grade was added. The products were separated and analyzed using a HPLC-MS system consisting of a shim-pack prep ODS column (150 × 4.6 mm, 5 mm), coupled to an Esquire ESI-MS spectrometer. The product that was characterized as POPC hydroperoxide was eluted during 7 min in a 1 mL $min^{-1}$ flux and resulted in *m*/*z* 792.7.

**Preparation of giant unilamellar vesicles.** The standard electroformation method[24] has been used throughout this study, to prepare giant unilamellar vesicles (GUVs). Non oxidized GUVs of POPC or DOPC were prepared from mixtures of the lipid with different fractions of sensitizer [0.03% mol to 2% mol]. GUVs of pure POPC–OOH or mixtures of 50/50

POPC/POPC–OOH that did not contain any photosensitizer were also prepared. Briefly, 5 μL of a 1 mg $mL^{-1}$ pure lipid, lipid mixture, or lipid/Chlorin-12 chloroform solution was spread and dried on the surfaces of two conductive glasses coated with indium tin oxide (ITO), which were then separated by a 2 mm thick Sigillum wax frame (Vitrex, Denmark) with their conductive sides facing each other. This electroswelling chamber was filled with 0.1 M sucrose solution and connected to an alternating power generator at 1 V with a 10 Hz frequency for 4 h. The vesicle solution was removed from the chamber and diluted 5 times with a 0.1 M glucose solution. This created a sugar asymmetry between the interior and the exterior of the vesicles. The osmolarities of the sucrose and glucose solutions were measured with a cryoscopic osmometer Osmomat 030 (Gonotec, Berlin, Germany) and carefully matched to avoid osmotic pressure effects.

### 2.3 Experimental setup

**Observation and UV irradiation.** Irradiation and observation of giant unilamellar vesicles of DOPC or POPC decorated with a small fraction (0.03% mol to 2% mol) of Chlorin-12 were achieved under an optical microscope (TE2000, Nikon, Japan), using a ×60 water immersion objective. Vesicles were irradiated with light from the HBO 103 W Hg lamp of the microscope, with an excitation filter centered at 410 nm, and observed through a longpass filter of lower cutoff at 520 nm. The power density $P_w$ of the irradiation was measured by a standard actinometry method,[25] we found $P_w = 27 \pm 4$ kW $m^{-2}$. Observation of the vesicles without irradiation was performed in DIC mode. Please note that POPC–OOH and 50/50 POPC–OOH/POPC GUVs were identically observed in this mode. All images were taken with a digital camera (Hamamatsu EM-CCD, Japan) at a rate of 8 frames per second, and analyzed using homemade software.

**Micropipette: constant suction and modulus measurement.** Micropipettes were made from borosilicate glass capillary GC100-15 tubing (Harvard apparatus Ltd., Kent, UK) using a pipette puller (Sutter instruments). A homemade microforge was used to tune their inner diameter to about 5 μm. Pipettes were coated with β-casein and then filled with the isosmotic glucose solution. The pipette was then driven in the observation field and brought in contact with a GUV. A negative suction pressure $P$ was applied through the pipette, thanks to a hydrostatic device. The suction pressure leads to a deformation of the vesicle corresponding to an added membrane tension $\sigma$. The device allows building the well known tension *versus* area expansion curve[26] from which both bending modulus $k_c$ and stretching modulus $K_A$ can be extracted. For non-oxidized vesicles we measured $K_A = 200 \pm 20$ mN $m^{-1}$ for both DOPC and POPC, in agreement with published data.[27] We have also characterized the stretching modulus $K_A$ of POPC–OOH membranes and of 50/50 POPC/POPC–OOH membranes prepared as explained above using the electroformation method. Furthermore, we also used our micropipette device to impose a constant tension of 0.7 mN $m^{-1}$, *i.e.* a value corresponding to the transition between the bending and stretching regimes where most of the area hidden in the thermal fluctuations is unfolded, to individual Chlorin-12 containing POPC or DOPC GUVs during continuous light irradiation. This led to an increase of the GUV membrane area with irradiation time, which could easily be followed and controlled. Some of these irradiation experiments were driven through long times, *i.e.* up to saturation of whether the membrane area increase, or the fluorescence bleaching, while in other experiments, we stopped the irradiation when a desired increase of membrane area was reached, corresponding to a given degree of membrane peroxydation. For this last type of experiment, the GUV was then submitted to the usual suction experiment, *i.e.* we built the usual tension *versus* area expansion curve and extracted the GUV's $K_A$ modulus.

## 3 Results and discussion

### 3.1 Molecular area increase and singlet oxygen production

Under irradiation, the photosensitizer Chlorin-12 generates singlet oxygen species $^1O_2$ that react with the chain double bonds, leading to the formation of the hydroperoxide –OOH group at positions 9 or 10 along the carbon chain.[10,11] Migration of this hydrophilic group to the bilayer–water interface results in a larger average molecular area per amphiphile as depicted in Fig. 2. Lipids with saturated chains such as DMPC do not exhibit area increase, see ESI.†

We measure concomitantly the increase of the vesicle bilayer area and the production of singlet oxygen with the micropipette setup coupled to an epi-fluorescence microscope. Under

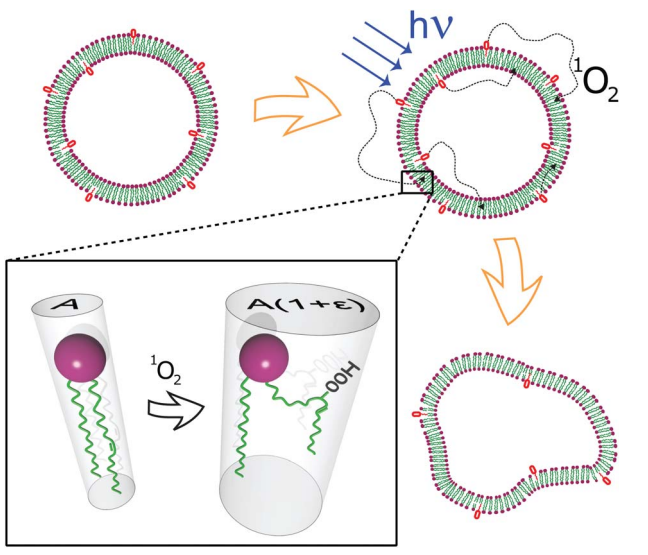


Fig. 2 Lipid and membrane transformations induced by hydroperoxidation. Irradiation of a vesicle decorated with the anchored photosensitizer Chlorin-12 generates singlet oxygen species $^1O_2$ that induce, under a constant irradiation, an increasing amount of oxidized lipids. Following a reaction with the $^1O_2$ moiety, the double bond in the unsaturated lipid tail of each lipid is converted into the organic hydroperoxide group –OOH. Its migration to the bilayer surface leads to a relative increase $\varepsilon$ of the average molecular area of the oxidized lipid. As the total area of the GUV bilayer expands, the membrane displays phenomena characteristic of membrane area increase,[28] such as enhanced fluctuations followed by bud and tube formation, as shown also in ESI Movie S1.†

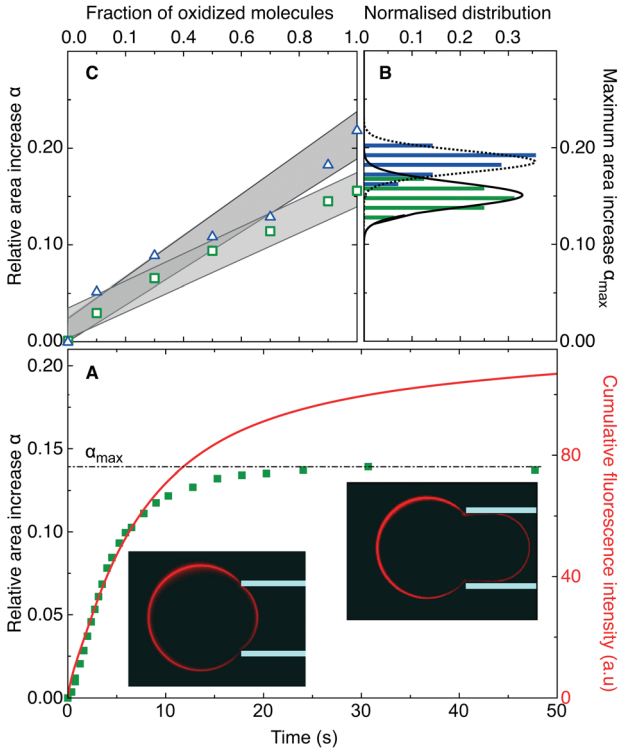


Fig. 3 Area expansion for unsaturated lipid membranes in Giant Unilamellar Vesicles. (A) Relative area increase (left *Y*-axis) as a function of time for an irradiated POPC vesicle containing 2% mol of the anchored photosensitizer Chlorin-12 (■). The relative area expansion was measured in a micropipette suction setup, as shown in the snapshot insets, at a constant membrane tension of 0.7 mN m$^{-1}$. The full curve (right *Y*-axis) shows in arbitrary units the cumulative light intensity emitted by the irradiated photosensitizers up to time *t*. The error bars are smaller than the symbol size. See also ESI Movie S2.† (B) The histograms represent the distribution of values for the relative increase in molecular area of POPC and DOPC lipids in GUV bilayers. Plateau values were extracted from full hydroperoxidation experiments performed on 14 vesicles of DOPC and 16 of POPC. The curves represent Gaussian fits. The average values are 15.6% for POPC and 19.1% for DOPC. (C) Values for the relative area increase for POPC (□) and DOPC (△) as a function of the fraction of oxidized lipids, computed from the Single Chain Mean Field theory described in the text.

irradiation at constant intensity and constant suction pressure, a growing amount of membrane is sucked into the micropipette as depicted in Fig. 3A, where the squares show results for the relative area increase of a typical POPC vesicle with 2% mol of Chlorin-12, see also ESI Movie S2.† After an initial increase, the relative area expansion reaches for this particular experiment a plateau around 14%. The full line in the figure displays the cumulative light intensity emitted by the photosensitizers up to time *t*, in arbitrary units. The cumulative intensity increases sub-linearly with time, due to Chlorin-12 bleaching. However, the area expansion curve reaches its plateau before the cumulative intensity curve saturates, showing that under these conditions all lipids have been converted into their hydroperoxide form before all the probes have been bleached. Full conversion is further supported by mechanical data presented below. Fig. 3B displays values for the relative molecular area increase extracted from experiments performed under full conversion conditions. The average values extracted from Gaussian fits are 15.6% for POPC and 19.1% for DOPC. An increase in the molecular area has also been observed for lipids hydroperoxidized at the water–air interface, as discussed in the ESI.†

We computed also from Single Chain Mean Field (SCMF) theory, as discussed in the ESI† section, the relative area increase as a function of the fraction of oxidized molecules. Fig. 3C displays numerical results for the relative area increase for POPC (□) and DOPC (△), in agreement with our experimental findings.

Given the known irradiation power, sensitizer cross-section for light absorption and quantum yield for $^1O_2$ production, measured by infrared experiments at 1270 nm in liposomal solutions, our experiments allow us also to quantitatively measure the number of singlet oxygen species generated by the anchored Chlorin-12 probes, provided that one uses low enough molar fractions of photosensitizers to preclude self-quenching effects. Under these conditions, prevailing in our case for photosensitizer molar fractions smaller than 0.1% mol of Chlorin-12, the emitted fluorescence intensity and the amount of generated $^1O_2$ species are proportional to probe density.

Fig. 4 shows typical results for a POPC vesicle with 0.03% mol of Chlorin-12. The squares in the figure correspond to the fraction of oxidized lipids obtained by dividing the measured values of relative area expansion by the average values of the corresponding plateaus measured above. Under the experimental conditions of Fig. 4, each photosensitizer produces roughly an average of 740 $^1O_2$ molecules per second. However, photobleaching strongly reduces $^1O_2$ production and in one

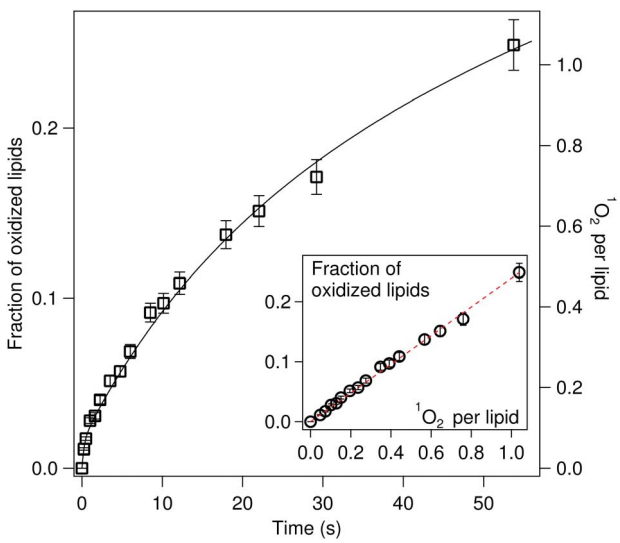


Fig. 4 Fraction of hydroperoxidized lipids (□, left *Y*-axis) as a function of time for an irradiated POPC vesicle containing 0.03% mol of the anchored photosensitizer Chlorin-12. The full curve (right *Y*-axis) shows the cumulative number of $^1O_2$ per lipid produced in time *t*. The efficiency of the reaction, measured by the number of $^1O_2$ species required to hydroperoxidize each POPC unsaturated bond can be read from the ratio of the scales in the left and right *Y*-axis or, alternatively, by the slope of the curve in the inset where the striking proportionality between oxygen production and lipid peroxidation is demonstrated.

minute each bilayer lipid is exposed on average to one $^1O_2$ species. The full line in the figure shows the cumulative number of singlet oxygen species per lipid generated in time $t$ in this experiment. The inset of Fig. 4 demonstrates the striking proportionality between singlet oxygen production and area increase, allowing to extract, from the slope of the curve, the efficiency $\eta$ of the reaction, as the fraction of generated $^1O_2$ species that oxidize one unsaturated bond. Efficiency values obtained from an average over three different experiments give $\eta_{POPC} \simeq 0.21 \pm 0.03$. Similar measurements performed on giant vesicles made from DOPC lipids provide comparable values $\eta_{DOPC} \simeq 0.19 \pm 0.01$.

The efficiency values for the reactions between the double bonds and the $^1O_2$ species were obtained here from a two-dimensional distribution of photosensitizers. A comparison with the bulk reaction constants from the literature[29] can nevertheless be attempted by extracting a second order reaction constant from the ratio between the density of hydroperoxidized groups and the product of the local densities of singlet oxygen and unsaturated bonds, as further detailed in the ESI† section. We get a reaction constant $k_{HP} \simeq 3 \times 10^6\ M^{-1}\ s^{-1}$, in close agreement with literature values for the binary reaction between $^1O_2$ and mono and di-saturated carbon chains in methanol.[29] Thus, the planar distribution of the anchored sensitizers does not appear to perturb the microscopic mechanisms of the photo-oxidation reaction. Instead, it dramatically reduces the total amount of photosensitizer required to fully oxidize the lipid double bonds. This can be better stressed by noticing that the singlet oxygen concentration $C_{SO}$ achieved in this anchoring geometry would require a bulk concentration $C_b$ of the same sensitizer of the order of $C_b = 0.5\Sigma\ell_D^{-1} \sim 25\ \mu M$, where $\Sigma$ is the number of photosensitizers per unit surface.

### 3.2 Mechanical modifications induced by lipid hydroperoxidation

Our experiments show that full conversion of the double bonds into their –OOH form does not compromise membrane integrity nor induces an increased permeability with respect to the sugar content in GUVs, thus allowing measurement of the stretching modulus of the membrane as a function of the lipid conversion degree from the native, non-oxidized form to their hydroperoxidized counterparts by the suction micropipette technique.[26,30] Fig. 5 displays the results obtained for both DOPC and POPC giant vesicles. Bilayers of native lipids exhibit stretching moduli $K_A$ of the order of 200 mN m$^{-1}$, in close agreement with published data for the same two systems.[27]

Fully oxidized bilayers of POPC have a stretching modulus of 50 mN m$^{-1}$ while DOPC bilayers with 35% of hydroperoxidized lipids have a stretching modulus of 150 mN m$^{-1}$, consistent with a linear variation of the modulus as a function of the conversion rate. The figure also shows stretching modulus measurements performed on giant vesicles electroformed from POPC–OOH, the hydroperoxidized form of POPC, that we have prepared independently, by standard methods described in the Experimental section, and from a 50/50 POPC/POPC–OOH mixture. Importantly, $K_A$ values for 100% POPC–OOH vesicles,

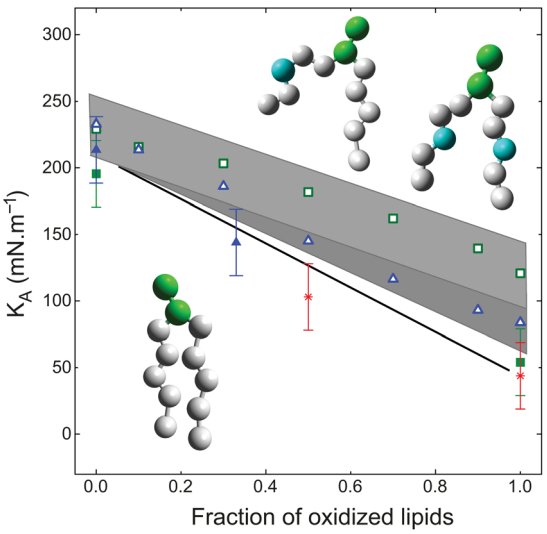


Fig. 5 The value of the membrane stretching modulus $K_A$ as a function of the fraction of oxidized lipids for DOPC (■), POPC (▲) and POPC–OOH (⋆) containing vesicles. The full straight line is a guide to the eye. The figure also reports values for POPC (□) and DOPC (△) stretching moduli as a function of the fraction of oxidized lipids, computed from the Single Chain Mean Field (SCMF) theory, see text. The grey area is an indication of uncertainties in the values from SCMF. An illustration of the cross-grained model with twelve beads used in SCMF is displayed in the figure. In this model hydroperoxidation changes the nature of the third bead in one (POPC) or two (DOPC) lipid tails.

of 50 mN m$^{-1}$, are similar to those of vesicles obtained by *in situ* hydroperoxidation, confirming that full conversion is reached under our irradiation conditions with 2% mol of probe content. Values for $K_A$ from a 50 : 50 mixture of POPC–OOH : POPC also support that the stretching modulus follows a linear variation with the fraction of POPC–OOH. Note that since *in situ* irradiation experiments are performed at a constant tension of 0.7 mN m$^{-1}$, a reduction of the elastic stretching constant influences also marginally the value of the relative area increase. This has also been accounted for as explained in the ESI† section.

In order to better understand the origin of the membrane transformations induced by hydroperoxidation, we also computed stretching moduli within Single Chain Mean-Field theory.[21,31] Since DOPC and POPC lipids have closely related molecular structures, the equilibrium properties of the assembled bilayers of DOPC and POPC were modelled with the same coarse-grained twelve-beads model sketched in Fig. 5. The head of lipids is composed of two hydrophilic beads and the two tails are composed of five hydrophobic beads. The model gives correct equilibrium properties of the bilayers, such as the thickness of the bilayer and of the hydrophobic core, the position of the head- and tail-groups, equilibrium area per lipid and the stretching modulus of the bilayer.[21] The oxidized lipid is modelled with the same twelve-bead model of Fig. 5, where the beads representing double bonds in the middle of the tails are replaced by a hydrophilic bead of the same radius as the beads composed of the head, but with two times weaker interactions with the solvent. As a result, the oxidized lipid POPC has one

hydrophilic bead in the tail, while the tails of the oxidized lipid DOPC have two hydrophilic beads. Introduction of hydrophilic beads in the tails of the lipids leads to structural changes of the bilayers and of their equilibrium properties. Fig. 5 displays results for the variation of the stretching modulus computed from SCMF theory as a function of the fraction of oxidized lipids, in good agreement with our experimental results.

The output from our simulations, along with simple theoretical arguments, indicate that the observed decrease of elastic modulus cannot be ascribed to a variation in membrane thickness only. If we represent the membrane as an elastic plate of a given Young's modulus $E$, the stretching modulus is proportional to the membrane thickness $h$, $K_A \sim Eh$.[32] At constant Young's modulus, one would require an unlikely decrease of the membrane thickness by a factor of four in order to explain the experimental observations. Instead, our SCMF results, consistent with all-atom simulations,[33] show only a slight membrane thinning, of roughly 10% for bilayers with 50% of hydroperoxidized lipids. Changes in the membrane mechanical properties are therefore a consequence of the transformation of the membrane's intimate structure. In particular, SCMF calculations show that the statistical distribution of the –OOH groups along the membrane thickness has a marked density at the lipid–water interface – see the ESI† section, consistent with the configurational transformation sketched in Fig. 2. This migration of the –OOH groups to the bilayer interface not only distorts the tail configurations resulting in a reduced cohesive energy of the hydrophobic bilayer core, but it also increases the hydrophilicity of the membrane water interface, reducing thus the interfacial tension costs associated with membrane stretching.[34] Importantly, the effect of adding hydrophilic groups to the middle of the hydrophobic chain is smaller than the effect of added moieties such as small surfactants or alcohols:[35] hydroperoxidation does soften the membrane, without however compromising its permeability or its integrity. This in turn, also points to less drastic changes than those leading for instance to interdigitation.[36]

# 4 Conclusions

Thus, understanding and controlling photo-oxidation mechanisms in self-assembled lipid bilayers require a quantitative microscopic picture describing the full chain of events, from the initial light absorption by the photosensitizers to the final modifications displayed by the oxidized membrane. A clear complete scenario for lipid hydroperoxidation emerges from our experimental geometry, where the spatial distribution of the oxidizing agents is controlled.

Singlet oxygen molecules are generated in the close vicinity of the bilayer, from where they start a random trajectory that penetrates the bilayer with probability close to unity. One out of five $^1O_2$ molecules will react with a double bond before it decays, leading to the formation of a –OOH group at positions 9 or 10 along the unsaturated chain. The hydrophilic character of the –OOH group increases its probability to settle at the lipid–water interface, and thus provides a driving force that changes the average chain conformation and the hydrophobic nature of the lipid–water interface. The resulting changes in chain conformation induce an increase of roughly 15–20% of the lipid molecular area, in agreement with our predictions from Single Chain Mean Field theory and consistent also with molecular simulations from Wong-Ekkabut *et al.*[33] The combined modifications of chain conformations and –OOH density at the lipid–water interface lead to a reduction by a factor of four of the bilayer stretching modulus. In spite of the modifications of the lipid molecular structure, the self-assembled bilayer is not destroyed, instead it retains its integrity and its impermeability with respect to sucrose or glucose.

The evaluation of lipid peroxidation from Giant Unilamellar Vesicles decorated with anchored sensitizers can address many of the open questions in this field and inspire new experiments. One could certainly explore for instance equilibrium shape transformations by inducing controlled changes in the surface to volume ratio.[37] Our results also allow quantifying the protective role of antioxidants and studying the mechanisms by which the unsaturated bonds can be protected from a reaction with singlet oxygen. Most importantly, this experimental geometry can also deal with lipid bilayers made from lipid mixtures and proteins, and thus contributes to elucidate how fundamental bio-relevant phenomena involved in lipid oxidation determine more complex mechanisms of cell function.

# Acknowledgements

This work is supported by grant #2012/50680-5, São Paulo Research Foundation (FAPESP) and is also part of a bilateral agreement USP-Cofecub (no. 2010.1.1049.43.9). RI and MSB also acknowledge Conselho Nacional de Pesquisa (CNPq) for research fellowships.

# References

1 B. N. Ames, M. K. Shigenaga and T. M. Hagen, *Proc. Natl. Acad. Sci. U. S. A.*, 1993, **90**, 7915–7922.
2 B. Halliwell and J. M. C. Gutteridge, *Free radicals in biology and medicine*, Oxford University Press, Oxford, 4th edn, 2007.
3 E. L. Crockett, *J. Comp. Physiol., B*, 2008, **178**, 795–809.
4 H.-P. Deigner and A. Hermetter, *Curr. Opin. Lipidol.*, 2008, **19**, 289–294.
5 R. S. Sohal and R. Weindruch, *Science*, 1996, **273**, 59–63.
6 C. J. Gomer, *Photodynamic therapy: methods and protocols*, Springer, New York, 1st edn, 2010, vol. 7651.
7 L. I. Grossweiner, L. R. Jones, J. B. Grossweiner and B. H. G. Rogers, *The science of phototherapy: an introduction*, Springer, Dordrecht, 2005.
8 M. Ochsner, *J. Photochem. Photobiol., B*, 1997, **39**, 1–18.
9 I. E. Kochevar, *Sci STKE*, 2004, **2004**, pe7.
10 H. Sies, *Angew. Chem., Int. Ed. Engl.*, 1986, **25**, 1058–1071.
11 S. P. Stratton and D. C. Liebler, *Biochemistry*, 1997, **36**, 12911–12920.
12 D. A. Pratt, J. H. Mills and N. A. Porter, *J. Am. Chem. Soc.*, 2003, **125**, 5801–5810.
13 P. R. Ogilby, *Chem. Soc. Rev.*, 2010, **39**, 3181–3209.

 

14 A. F. Uchoa, K. T. de Oliveira, M. S. Baptista, A. J. Bortoluzzi, Y. Iamamoto and O. A. Serra, *J. Org. Chem.*, 2011, **76**, 8824–8832.
15 F. M. Megli and K. Sabatini, *Chem. Phys. Lipids*, 2003, **125**, 161–172.
16 W. Caetano, P. S. Haddad, R. Itri, D. Severino, V. C. Vieira, M. S. Baptista, A. P. Schröder and C. M. Marques, *Langmuir*, 2007, **23**, 1307–1314.
17 R. F. Jacob and R. P. Mason, *J. Biol. Chem.*, 2005, **280**, 39380–39387.
18 A. G. Ayuyan and F. S. Cohen, *Biophys. J.*, 2006, **91**, 2172–2183.
19 J. Heuvingh and S. Bonneau, *Biophys. J.*, 2009, **97**, 2904–2912.
20 H. Mojzisova, S. Bonneau, P. Maillard, K. Berg and D. Brault, *Photochem. Photobiol. Sci.*, 2009, **8**, 778–787.
21 S. Pogodin and V. A. Baulin, *Soft Matter*, 2010, **6**, 2216–2226.
22 M. T. Jarvi, M. J. Niedre, M. S. Patterson and B. C. Wilson, *Photochem. Photobiol.*, 2006, **82**, 1198–1210.
23 M. C. Petty, *Langmuir–Blodgett films: an introduction*, Cambridge University Press, Cambridge, 1996.
24 M. Angelova and D. Dimitrov, *Faraday Discuss.*, 1986, **81**, 303–311.
25 C. G. Hatchard and C. A. Parker, *Proc. R. Soc. London, Ser. A*, 1956, **235**, 518–536.
26 E. Evans and W. Rawicz, *Phys. Rev. Lett.*, 1990, **64**, 2094–2097.
27 W. Rawicz, K. Olbrich, T. McIntosh, D. Needham and E. Evans, *Biophys. J.*, 2000, **79**, 328–339.
28 K. A. Riske, T. P. Sudbrack, N. L. Archilha, A. F. Uchoa, A. P. Schroder, C. M. Marques, M. S. Baptista and R. Itri, *Biophys. J.*, 2009, **97**, 1362–1370.
29 F. Wilkinson and J. Brummer, *J. Phys. Chem. Ref. Data*, 1981, **10**, 809–999.
30 J.-B. Fournier, A. Ajdari and L. Peliti, *Phys. Rev. Lett.*, 2001, **86**, 4970–4973.
31 S. Pogodin and V. A. Baulin, *Curr. Nanosci.*, 2011, **7**, 721–726.
32 L. Landau and E. Lifshitz, *Theory of Elasticity*, Pergamon Press, Oxford, UK, 3rd edn, 1986.
33 J. Wong-Ekkabut, Z. Xu, W. Triampo, I.-M. Tang, D. P. Tieleman and L. Monticelli, *Biophys. J.*, 2007, **93**, 4225–4236.
34 D. Marsh, *Biochim. Biophys. Acta*, 1996, **1286**, 183–223.
35 J. Häckl, U. Seifert and E. Sackmann, *J. Phys. II*, 1997, **7**, 1141–1157.
36 M. Kranenburg, M. Vlaar and B. Smit, *Biophys. J.*, 2004, **87**, 1596–1605.
37 J. Käs and E. Sackmann, *Biophys. J.*, 1991, **60**, 825–844.

**Supplementary Information**

# 1 Synthesis and characterization of the photosensitizer

The compound that we named Chlorin-12 is the second of the isomers characterized by $^1$H-NMR (see Fig.S1), COSY, ESI-MS and UV-Vis.

**$2^1$,$2^2$[*N*,*N*-dicarbonyl-*N*-(4-dodecylphenyl)]-8,12-bis[2-(methoxycarbonyl) ethyl]-2,7,13,17-tetramethyl-18-vinyl-$2,2^1,2^2,2^3$-tetrahydrobenzo[*b*]porphyrin.** $^1$H NMR ($CDCl_3$, 500 MHz), $\delta$ (ppm): -2.45 (br s, 2H, H-21 and H-23); 0.9-1.27 (m, *p*-alkyl group); 2.08 (s, 3H, $CH_3$-$2^5$), 3.17 (t, 2H, $J$ = 8.0 Hz, H-$12^2$), 3.21 (t, 2H, $J$ = 8.0 Hz, H-$8^2$); 3.42 (s, 3H, $CH_3$-$13^1$); 3.47 (s, 3H, $CH_3$-$7^1$); 3.45-3.48 (m, 2H, H-$2^{3\alpha}$ and H-$2^{3\beta}$); 3.61 (s, 3H, $CH_3$-$17^1$), 3.91-3.95 (m, 1H, H-$2^2$) 3.65 and (s, 3H, $12^4$); 3.66(s, 3H, $8^4$);4.18 (t, 2H, $J$ = 8.0 Hz, H-$12^1$); 4.32 (t, 2H, $J$ = 8.0 Hz, H-$8^1$); 4.65 (d, 1H, $J$ = 8.5 Hz, H-$2^1$); 6.10 (dd, 1H, $J$ = 11.5 and 1.5 Hz, H-$18^{2\alpha}$); 6.33 (dd, 1H, $J$ = 18.0 and 1.5 Hz, H-$18^{2\beta}$); 6.99-7.01 (m, 2H, H-$2^9$ and $2^{13}$); 7.41 (t, $J$ = 5.0 Hz, 1H, H-$2^4$); 7.73-7.70 (m, 2H, H-$2^{10}$ and H-$2^{12}$); 8.13 (dd, 1H, $J$ = 18.0 and 11.5 Hz, H-$18^1$); 9.26 (s, 1H, H-5); 9.28 (s, 1H, H-20); 9.68 (s, 1H, H-10), 9.74 (s, 1H, H-15).

**ESI-MS-TOF**, m/z 933.5321 calculated for $C_{58}H_{70}N_5O_6^+(MH^+)$; found 933.5329.

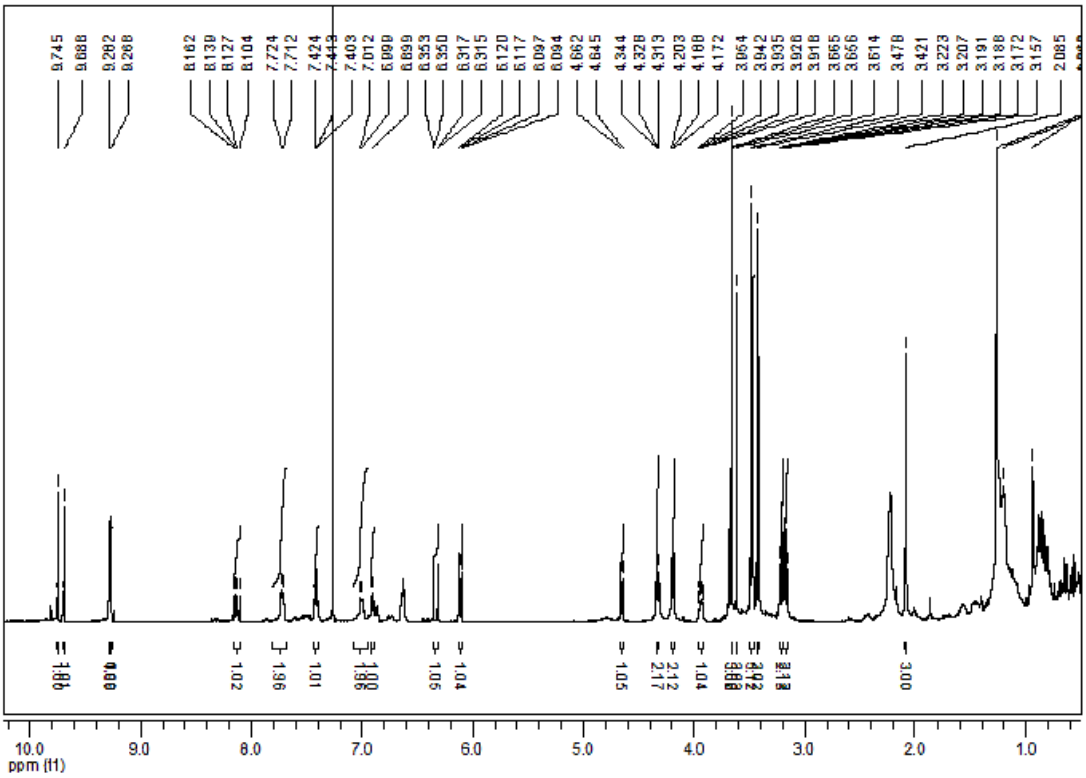


Figure S1: $^1$H-NMR (500 MHz) in $CDCl_3$ of Chlorin-12.

# 2 Langmuir monolayer

We performed Langmuir isotherms on pure POPC and pure POPC-OOH molecules (see Fig. S2). Precautions were taken in order to avoid oxidation of the monolayers exposed to laboratory air by working under controlled $N_2$ atmosphere. POPC-OOH shows clearly values of area per molecule (APM) which are larger than POPC.

Defining $\Delta A/A$ as

$$\frac{\Delta A}{A} = \frac{APM_{POPC-OOH} - APM_{POPC}}{APM_{POPC}}, \tag{1}$$

we measure $\Delta A/A \sim 50\% at low pressure$, in agreement with the observations of van den Berg et al. [1] who compared PLPC monolayers with PLPC-OOH monolayers. Fig. S3 represents the

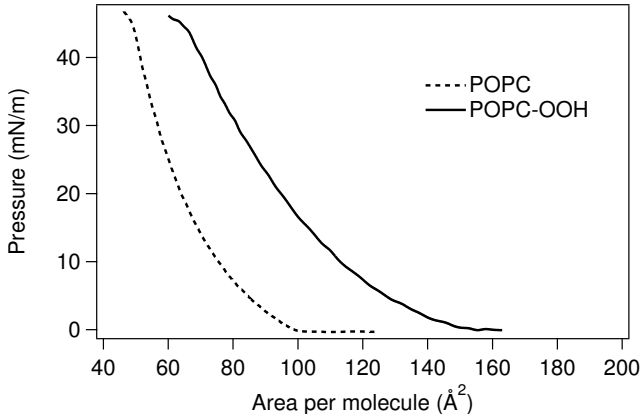


Figure S2: Langmuir isotherms at 20°C of monolayers made of mixtures of POPC (dashed line) and of the hydroperoxidized form POPC-OOH (full line).

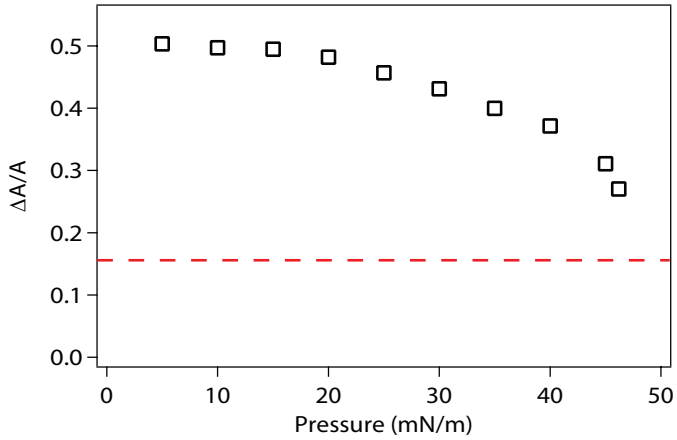


Figure S3: $\Delta A/A$ as a function of the pressure $\Pi$ (□). The dashed line corresponds to the relative area difference between POPC and POPC-OOH in bilayers.

evolution of $\Delta A/A$ as a function of the surface pressure $\Pi$. This relative area difference decreases as the pressure increases. For the maximum pressure that we can achieve, $\Delta A/A$ decreases to 27%. Thus, whatever the pressure, $\Delta A/A$ remains larger than the relative area increase measured in fully oxidized POPC bilayers ($\sim 15\%$).

Despite intrinsic structural differences between monolayers and bilayers, it has been shown that for a certain lateral pressure, around 30-35 mN/m, the hydration state of both monolayer and bilayer systems is identical and structural parameters of these systems are comparable [2,3]. The use of monolayers to predict bilayer properties seems reasonable provided that bilayers can be pictured as two back-to-back monolayers interacting non-specifically as two slabs [4]. Depending on the properties one focuses on, the monolayer / bilayer equivalence occurs at different pressures. In the case of relative area increase between POPC and its hydroperoxidized form POPC-OOH, even if there is no pressure value that allows to reach the monolayer / bilayer equivalence, our results clearly show a larger area per molecule of the hydroperoxidized form of the lipids in qualitative agreement with area increase in the bilayers.

# 3 Experiments analysis

## 3.1 Control experiments

### 3.1.1 Start-Stop experiments

We performed start-stop experiments on the decorated GUVs, hold by the micropipette, by irradiating the sample for 10 seconds, and then observing the vesicles under the DIC observation mode for 15 seconds. No delayed effects could be detected, either after stopping or after restarting irradiation. Under our conditions, there is thus an instantaneous response of the vesicle area expansion to the irradiation.

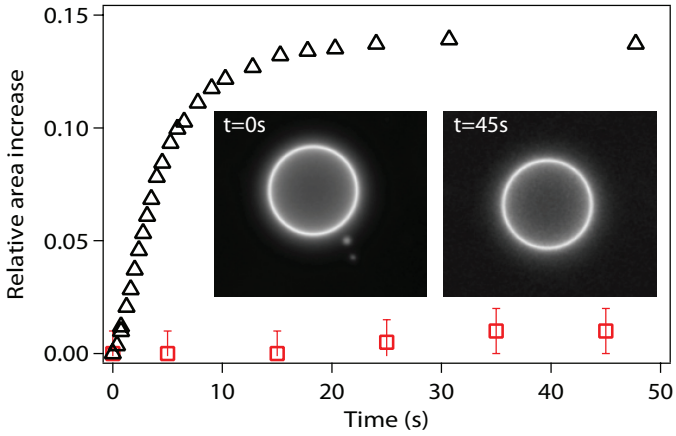


Figure S4: Evolution of the area increase in a DMPC vesicle with 1% of Chlorin-12 (□) under light irradiation and the corresponding fluorescence images, compared to the POPC vesicle showed before (△). Saturated lipids are not oxidised by singlet oxygen.

### 3.1.2 Singlet oxygen does not oxidise saturated lipids

We have checked that oxidation phenomena is not present for lipid chains without unsaturated bonds. We prepared GUVs made of DMPC (a lipid with two saturated chains of 14 carbons) incorporating also 1% of Chlorin-12. The liquid/gel transition temperature of DMPC is 23°C. Thus, vesicle formation has been performed in an oven at 28°C. Irradiation of the DMPC giant vesicles showed no membrane transformations. Fluorescence from Chlorin-12 molecules followed the same time evolution due to bleaching, but no enhanced fluctuations or tube/bud formation was observed. A simple image analysis, using a $2\pi$ average radial profile was enough to extract the vesicle area evolution. Fig. S4 clearly shows no area increase.

## 3.2 Correction of the apparent area increase

During our irradiation experiments one measures an overall increase of the apparent surface area of a GUV submitted to a constant membrane tension, applied through the micropipette device. At constant tension, a measure of area increase due to lipid peroxidation is also perturbed by the changes of the stretching modulus of the membrane. Here, we correct for such (minor) perturbations by considering first the Evans-Helfrich equation for $\alpha$, the apparent area increase of a membrane submitted to a given tension $\sigma$, as a function of its constitutive mechanical parameters, the bending modulus $k_c$ and the elastic modulus $K_A$

$$\alpha = \frac{k_B T}{8\pi k_c} \ln(\frac{\sigma}{\sigma_0}) + \frac{\sigma}{K_A}, \tag{2}$$

where $\sigma_0$ is a constant. In the present case, the membrane is submitted to a constant tension $\sigma$, and after a time $t$ of illumination, a fraction $x_{ox}$ of the lipids have been peroxidized, leading to a relative area increase $x_{ox}\epsilon$, where $\epsilon$ is the relative molecular area increase, and to a decrease of both $k_c$ and $K_A$. We have measured a linear decrease of $K_A$ with $x_{ox}$ and noticed, without being able for technical reasons to measure it precisely, a decrease in $k_c$. Then, Eq. (2) becomes, after an irradiation time $t$

$$\alpha(x_{ox}) = \frac{k_B T}{8\pi k_c^{\text{eff}}(x_{ox})} \ln(\frac{\sigma}{\sigma_0}) + \frac{\sigma}{K_A^{\text{eff}}(x_{ox})} + x_{ox}\epsilon \tag{3}$$

with $K_A^{\text{eff}}(x_{ox}) = K_A(1 - x_{ox}) + K_A^{ox} x_{ox}$, where $K_A^{ox}$ is the bending modulus of a completely peroxidized membrane that we have measured. The maximum error is expected for a fully peroxidized membrane. Assuming a decrease of a factor of four for $k_c$, $k_c^{ox} = 0.25\ k_c$, similar to that measured for $K_A$, $K_A^{ox} = 0.25\ K_A$, it follows that the error on the relative area increase $\epsilon(x_{ox} = 1)$, is less than 1% for a membrane submitted to a tension $\sigma$ =0.7 mN m$^{-1}$. Notice that the relative error remains smaller than one percent if $k_c^{ox}$ assumes values in the range $0.25\ k_c < k_c^{ox} < k_c$.

## 3.3 Data Analysis

GUVs decorated with various surfaces concentrations of Chlorin-12 under continuous irradiation at 410 nm, show a typical fluorescence intensity decrease due to photobleaching. We computed

the cumulative intensity as the integral over time of the fluorescence signal. For a given quantum yield for $^1O_2$ production $\phi_\Delta$, the cumulative fluorescence is thus directly proportional to the number of $^1O_2$ species produced since the beginning of the irradiation. In the absence of bleaching, the cumulative intensity should grow linearly with time. The decrease of light intensity associated with photobleaching results in a sublinear variation of the cumulative light intensity with time. The constant of proportionality between emitted light intensity and singlet oxygen generation can be computed by noticing that the rate of singlet oxygen production $Q$ is given by [5] $Q = \phi_\Delta \lambda P_w \sigma / hc$, where $\lambda$ is the wavelength of the irradiation light (410 nm), $P_w$ the power density, $\sigma$ the cross section of absorbance, $h$ the Planck's constant, and $c$ the speed of light. For Chlorin-12, $\phi_\Delta = 0.63$ and $\sigma(410\text{ nm}) = 2.1$ Å$^2$. Thus, in our setup, each non-bleached Chlorin-12 has a production rate $Q$=740 molecules of $^1O_2$ per second. The associated relative area increase was measured on each vesicle by a direct analysis of the vesicle dimensions on the fluorescence images, for different irradiation times and further corrected for $K_A$ decrease as explained above.

# 4 $^1O_2$ Sources, diffusion and reactions

## 4.1 Computing $^1O_2$ distribution

The concentration of $^1O_2$ near the plane of anchored sensitizers can be computed by solving the reaction-diffusion equation for the distribution of $^1O_2$ species:

$$\frac{\partial C_{SO}}{\partial t} = D\frac{\partial^2 C_{SO}}{\partial z^2} - \frac{C_{SO}}{\tau} + Q\Sigma\delta(z-b) \tag{4}$$

where $C_{SO}$ is the singlet oxygen concentration profile, $D$ the diffusion coefficient, $z$ the distance away from the membrane, $\tau$ the $^1O_2$ lifetime, $Q$ the rate of $^1O_2$ generation per sensitizer molecule and $\Sigma$ the number of sensitizers per unit area. $b$ is the distance from the $^1O_2$ generation plane from the membrane, of order of a fraction of nanometer. Eq. 4 supposes that singlet oxygen reactions with the unsaturated bonds only marginally perturb the distribution, a full description would require a sink term located at the average (negative) height of the double bond plane. The stationary solution of Eq. 4 reads

$$C_{SO}(z) = \frac{Q\tau\Sigma}{2\ell_D}\exp\{-\frac{z}{\ell_D}\}. \tag{5}$$

Close to the generating wall there is thus a concentration of singlet oxygen given by

$$C_{SO}(z=0) = 0.5Q\tau\Sigma\ell_D^{-1}. \tag{6}$$

Under our irradiation conditions and for a Chlorin-12 molar fraction of 0.03 %, where $Q = 740\text{ s}^{-1}$, $\ell_D = 100$ nm, $\tau = 4$ $\mu$s, we have $C_{SO}(z=0) = 12$ nM. It is also worth stressing that the planar localization of the sensitizers might lead to oxygen depletion if the sensitizer surface density $\Sigma$ is too large. A higher bound value for $\Sigma_{\max}$ can be estimated based on the comparison between the concentration of singlet oxygen at the surface $C_{SO}(z=0)$ and the concentration of molecular oxygen in solution $C_{O2}$, giving $\Sigma_{\max} = 2C_{O2}\ell_D Q^{-1}\tau^{-1}$ and a maximum sensitizer fraction $f_{\max} = \Sigma_{\max} S_0$ where $S_0$ is the area of one lipid molecule. Under our conditions where $S_0$ =0.65 nm$^2$, and $C_{O2}$ =250 $\mu$M, we get $f_{\max}$ of order unity. In our case, where $f_{\max} \ll 1$, $^1O_2$ generation should thus not be limited by oxygen depletion effects.

## 4.2 Inhomogeneities in singlet oxygen distribution

The smallest average time interval between two successive $^1O_2$ generation events being, under our irradiation conditions, of order of 1.4 ms, the sensitizer diffuses in this interval over a typical distance of 20 nm. The distance between two probes is explored in 7 ms by the photosensitizer diffusive motion, corresponding to 5 emission events; during the time of the experiment, which is of order of one minute, each photosensitizer diffuses thus over distances one hundred times larger than the inter-probe length further contributing to an homogeneous distribution of $^1O_2$ species. These homogenizing factors are even stronger for the surface densities of the samples with high probe fractions such as the 2 % mol case shown in the main text, where the average distance between sensitizers is smaller than 10 nm. However, in this denser case, the average distance between sensitizers is comparable with the length below which self-quenching becomes significant [6], we thus confined our quantitative efficiency measurements to samples with lower probe densities, as discussed in the next paragraph.

### 4.3 Equivalent bulk constants for the hydroperoxidation reaction

Photosensitizers generate an average concentration of $^1O_2$ species close to the membranes given by $C_{SO} = 0.5\Sigma Q\tau\ell_D^{-1}$, where $Q$ is the number of $^1O_2$ generated per photosensitizer by unit time, $\Sigma$ the number of photosensitizers per unit surface and $\tau$ the $^1O_2$ lifetime. The factor 0.5 relies on the assumption that $^1O_2$ molecules distribute evenly on both sides of the probe plane. In a binary reaction between $^1O_2$ species at a concentration $C_{SO}$ and double bonds of concentration $C_{DB}$ one creates $k_{HP}C_{DB}C_{SO}$ hydroperoxide species per unit time $dC_{HP}/dt = k_{HP}C_{SO}C_{DB}$. Associating $m$, the initial slope of the curve in Fig. 4 (main text), with the value for the relative rate production of -OOH groups, $m = C_{DB}^{-1}dC_{HP}/dt|_{t=0}$ one has $k_{HP} = m \times C_{SO}^{-1}$. For the case of Fig. 4 in the main text, $m = 0.036$. With $Q = 740$ s$^{-1}$, $\ell_D = 100$ nm, $\tau = 4$ $\mu$s and $\Sigma = 4.7 \times 10^{-4}$ nm$^{-2}$, this leads to the reaction constant value $k_{HP} \simeq 3 \times 10^6$ M$^{-1}$s$^{-1}$.

## 5 Single Chain Mean Field theory

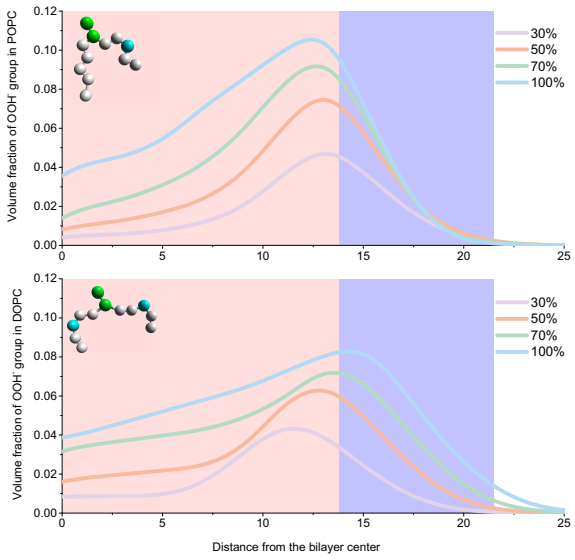


Figure S5: Averaged position of the oxidized beads in POPC bilayer (top) and DOPC bilayer (bottom) as a function of the distance from the center of the bilayer for different rates of oxidation. Rose band corresponds to the hydrophobic core of the bilayer, while blue band corresponds to the heads region. Typical configurations of the oxidized lipids are shown in the inset.

Lipid molecules are modeled within the Single Chain Mean Field theory [7]. This theory is shown to describe adequately equilibrium and mechanical properties of lipid bilayers using coarse-grained models for lipid molecules [7]. Since mechanical and equilibrium properties of DOPC and POPC lipid bilayers, such as thickness, compressibility and the area per lipid are very close to each other, we describe both DOPC and POPC lipid bilayers using unique 10-beads model shown in Fig. 5 of main text. The oxidized DOPC and POPC molecules are described with the same set of parameters as non-oxidized lipids, but the central hydrophobic bead of the tail (grey), which corresponds to the double bond, is replaced by a hydrophilic bead (cyan), which has interactions with solvent two times less than the beads of the heads (green) (see Fig. S5). Our SCMF calculations have shown that more hydrophilic OOH group migrates closer to the surface, forming a kink in the tails. The oxidized beads stay at the border between hydrophobic core and the heads region. These groups, in turn, distort the bilayer, preventing close packing of neighboring tails, which is probably the main effect of oxidation. Although the peak of average position of OOH groups is slightly displaced to the surface of the bilayer (Fig. S6), some OOH groups can be found outside of the bilayer (Fig. S6).

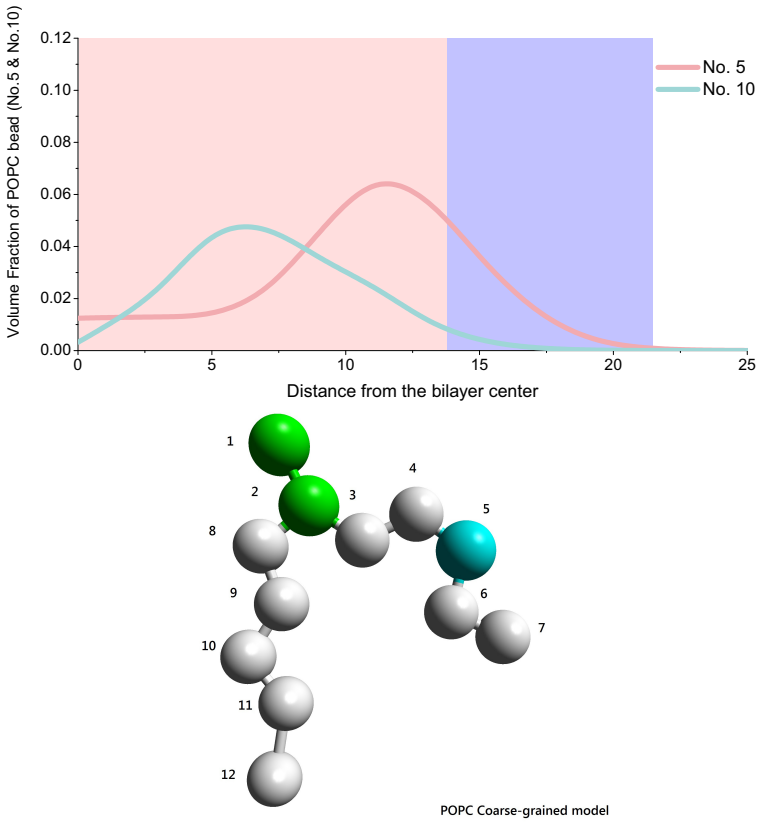


Figure S6: Averaged position of oxidized OOH group (bead N° 5) and symmetrical carbon group (bead N° 10) of POPC oxidized lipid in the bilayer.

# References

[1] J J van den Berg, J A Op den Kamp, B H Lubin, and F A Kuypers. Conformational changes in oxidized phospholipids and their preferential hydrolysis by phospholipase a2: a monolayer study. *Biochemistry*, 32(18):4962–7, May 1993.

[2] J. Brewer, J. Bernardino de la Serna, K. Wagner, and L. A. Bagatolli. Multiphoton excitation fluorescence microscopy in planar membrane systems. *Biochimica and Biophysica Acta*, 1798:1301Ð1308, 2010.

[3] D Marsh. Lateral pressure in membranes. *Biochim Biophys Acta*, 1286(3):183–223, Oct 1996.

[4] J.F. Nagle and S. Tristram-Nagle. Structure of lipid bilayers. *BBA Biomembranes*, 1469:159–195, 2000.

[5] N. A. Busch, M. L. Yarmush, and M. Toner. A theoretical formalism for aggregation of peroxidized lipids and plasma membrane stability during photolysis. *Biophys J*, 75(6):2956–2970, Dec 1998.

[6] Joseph R. Lakowicz. *Principle of fluorescence spectroscopy*. Springer, 3rd edition, 2006.

[7] Sergey Pogodin and Vladimir A. Baulin. Coarse-grained models of phospholipid membranes within the single chain mean field theory. *Soft Matter*, 6(10):2216–2226, 2010.